Alexandria Engineering Journal (2015) 54, 1067–1075

HOSTED BY

Alexandria University

Alexandria Engineering Journal

www.elsevier.com/locate/aej
www.sciencedirect.com

ORIGINAL ARTICLE

Sliding mode direct power control of RSC for DFIGs driven by variable speed wind turbines

E.G. Shehata

Electric Engineering Dept., Faculty of Engineering, Minia University, El-Minia, Egypt

Received 18 November 2014; revised 13 May 2015; accepted 6 June 2015
Available online 3 July 2015

KEYWORDS

Doubly fed induction generators;
Direct power control;
Total sliding mode controller

Abstract In spite of its several advantages, a classic direct power control (DPC) of doubly fed induction generators (DFIGs) driven by variable speed wind turbines has some drawbacks. In this paper, a simple and robust total sliding mode controller (TSMC) is designed to improve the classical DPC performance without complicating the overall scheme. The TSMC is designed to regulate the DFIG stator active and reactive powers. Two integral switching functions are selected for describing the switching surfaces of the active and reactive powers. Reaching phase stability problem of the classical sliding mode controller is avoided in the proposed TSMC. Neither current control loops nor accurate values of machine parameters are required in the proposed scheme. In addition, axes transformation of the stator voltage and current are eliminated. The grid side converter is controlled based on DPC principle to regulate both DC-link voltage and total reactive power. The feasibility of the proposed DPC scheme is validated through simulation studies on a 1.5 MW wind power generation system. The performance of the proposed and conventional DPC schemes is compared under different operating conditions.

1. Introduction

Doubly Fed induction generators have been widely used for large scale wind generation systems. Control and operation of DFIGs have been the subject of intense research during last few years. Wind farms based on the DFIGs with converters rated at 25–30% of the generator rating are becoming increasingly popular. Compared with wind turbines using fixed speed, the DFIGs based wind turbines offer not only advantages of variable speed operation and four-quadrant active and reactive power capabilities, but also lower converter cost and power losses [1]. Various control algorithms have been proposed for studying the behavior of DFIG based wind-turbine system during normal operation. Most existing models widely used a conventional vector control based on a stator flux orientation (SFO) [2] or a stator voltage orientation (SVO) [3]. A decoupled control of the instantaneous stator active and reactive powers has been achieved by regulating the decomposed rotor currents using proportional–integral (PI) controllers. However, PI-controllers performance is highly dependence on tuning of parameters and accurate tracking of angular information of stator flux/voltage. Moreover, the vector or field oriented control schemes need accurate values of machine parameters and rotor speed.

E-mail address: emadgameil@mu.edu.eg
Peer review under responsibility of Faculty of Engineering, Alexandria University.

http://dx.doi.org/10.1016/j.aej.2015.06.006
1110-0168 © 2015 Faculty of Engineering, Alexandria University. Production and hosting by Elsevier B.V.

Alternative approaches to field oriented control such as a direct self control (DSC) [4] and a direct torque control (DTC) [5] have been proposed for cage rotor induction machines. In these strategies, two hysteresis controllers, namely torque and flux controllers are selected to determine the inverter instantaneous switching state [6]. Similar to the DTC, a direct power control (DPC) of DFIG based wind turbine systems has proposed recently [6–15]. The instantaneous switching state of the rotor side converter is determined based on the stator active and reactive power errors. Thus, unlike existing DTC techniques, measurements are carried out at one terminal of the machine whereas the switching action is carried out at another terminal [6]. Since the rotor supply frequency may be very low, the rotor flux estimation can be significantly affected by the machine parameter variations. In [7], DPC strategy based on an estimated stator flux has been proposed. As the stator voltage is relatively harmonics free, the accuracy of the stator flux estimation can be guaranteed. However, an unfixed switching frequency is considered the main drawback of classical DPC. In [8], a modified DPC strategy was proposed based on SFO control with a constant switching frequency, where a reference rotor voltage was calculated based on the estimated stator flux, active and reactive powers and their errors. In [9], an active and reactive power proportional–integral controllers and space vector modulation technique (SVM) were combined to replace the conventional hysteresis controllers. For operation under unbalanced and harmonically grid voltage, different DPC algorithms were designed to overcome the bad effects under these conditions and improve the overall performance [10–15]. In [10], two resonant controllers were designed to regulate the active and reactive power without sequential decomposition involved. In [11], the electromagnetic torque oscillations at double supply frequency under unbalanced stator supply were eliminated. In [15], an improved DPC strategy of a wind turbine driven DFIGs connected to distorted grid voltage conditions was presented.

For robust and high performance DPC, a sliding mode controller (SMC) was studied in the literature [16–23]. It is an effective, high frequency switching control strategy for nonlinear systems with uncertainties. It can offer many good properties such as good performance against unmodeled dynamics, insensitivity to parameters variation, external disturbance rejection and fast dynamic response. A SMC was designed to control the RSC under normal abnormal grid voltage conditions [16–23]. In [16], an integral sliding mode controller was designed to regulate the electromagnetic torque and stator reactive power. SMC and fuzzy logic controller are combined to control doubly fed induction machines [17]. A discrete SMC is designed to regulate the real and reactive stator power of DFIG [18]. Sliding mode controller is proposed to regulate the stator active and reactive power under unbalanced and harmonically distorted grid voltage [20–23]. In [22], two sliding mode controllers are designed to determine directly the switching state of RSC and GSC under harmonically and unbalanced grid voltage conditions. However, the switching frequency of the two converters is variable and high chattering appears in the electromagnetic torque, DC-link voltage, stator and total powers waveforms. However, the reaching phase stability and chattering problem were not taken into account in the previous research.

In this paper, a coordinated direct power control of the RSC and grid side converter (GSC) is presented. The GSC is controlled based on DPC principle to regulate the DC-link voltage, total active and reactive power. Meanwhile, the RSC is controlled to regulate the stator active and reactive powers. To obtain high performance DPC, a simple and robust sliding mode controller is designed to control the RSC and regulate the stator active and reactive power. Two integral functions are selected to describe the switching surfaces for stator active and reactive power control. The total sliding mode controller is designed to avoid the reaching phase stability problem. The proposed scheme preserves the advantages of the classical DPC such as simplicity, less parameters dependence and fast response. In addition, axes transformation of the stator voltage or current is not required. The stability of the total sliding mode controller is proven using Lyapunov stability theorem. Finally, the proposed and conventional DPC [11] schemes performance is verified by the simulation study on 1.5 MW DFIG system under variation of wind speed, machine parameters and unbalanced grid voltage.

2. Maximum Power Point Tracking (MPPT) strategy

The output power of a wind turbine is given [24]:

$$P_m = c_P(\lambda,\beta)\frac{\rho A}{2}v_t^3 \tag{1}$$

where P_m is a mechanical output power of the turbine (W), c_P is a power coefficient, ρ is an air density (kg/m^3), A is a turbine swept area (m^2), v_t is a wind speed (m/s), λ is a tip speed ratio of the rotor blade tip speed to wind speed, and β is a blade pitch angle (°). A generic equation is used to model c_p (λ, β), based on the modeling turbine characteristics is:

$$c_P(\lambda,\beta) = c_1\left(\frac{c_2}{\lambda_i} - c_3\beta - c_4\right)e^{\frac{-c_5}{\lambda_i}} + c_6\lambda \tag{2}$$

The coefficients c_1 to c_6 of 1.5 MW wind turbine are [24]: $c_1 = 0.5176$, $c_2 = 116$, $c_3 = 0.4$, $c_4 = 5$, $c_5 = 21$ and $c_6 = 0.0068$. The maximum value of c_p ($c_{p\max} = 0.48$) is achieved for $\beta = 0°$ and for $\lambda = 8.1$. This particular value of λ is defined as the nominal value ($\lambda_{\_nom}$). The mechanical power P_m as a function of generator speed, for different wind speeds and blade pitch angle $\beta = 0°$, is illustrated in Fig. 1.

3. Dynamic model of DFIG

Fig. 2 shows the generalized equivalent circuit of a DFIG in a synchronous reference frame (d-q) rotating at an angular speed of ω_e [1]. The stator and rotor voltages are given, respectively, as follows:

$$\begin{aligned} V_s &= R_s I_s + \frac{d}{dt}\lambda_s + j\omega_e\lambda_s \\ V_r &= R_r I_r + \frac{d}{dt}\lambda_r + j\omega_s\lambda_r \end{aligned} \tag{3}$$

where ω_s is the slip angular speed ($\omega_s = \omega_e - \omega_r$), ω_r is the rotor angular speed, R_s and R_r are the stator and rotor resistances, respectively, I_s and I_r are the stator and rotor currents, respectively. The stator and rotor flux can be expressed as follows:

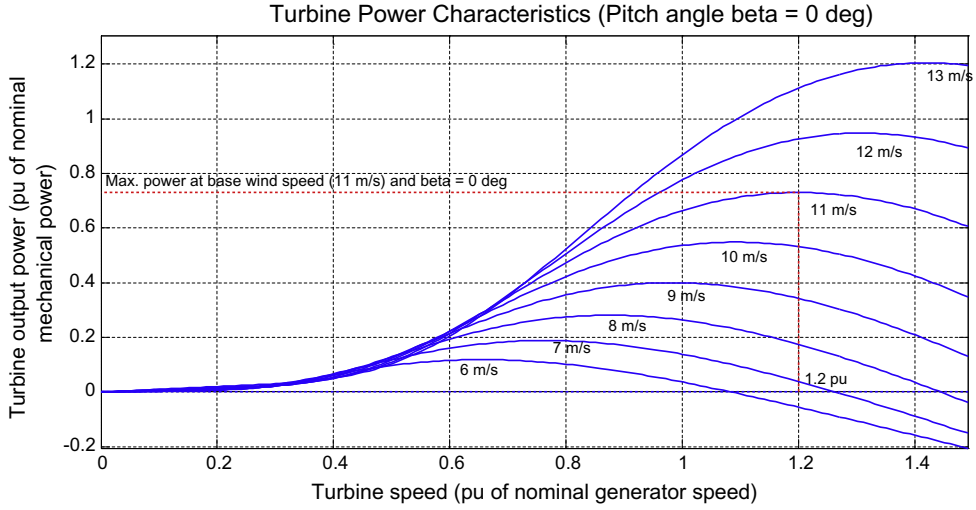

Figure 1 Turbine and tracking characteristic with pitch angle = 0°.

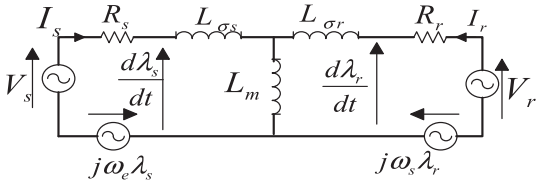

Figure 2 Equivalent circuit of a DFIG in a synchronous reference frame.

$$\begin{aligned}\lambda_s &= L_s I_s + L_m I_r \\ \lambda_r &= L_m I_s + L_r I_r\end{aligned} \tag{4}$$

where $L_s = L_{\sigma s} + L_m$ and $L_r = L_{\sigma r} + L_m$. L_m, $L_{\sigma s}$ and $L_{\sigma r}$ are the mutual inductance and the stator and rotor leakage inductances, respectively. According to (4), the stator current is given as

$$I_s = \frac{L_r\lambda_s - L_m\lambda_r}{L_s L_r - L_m^2} = \frac{\lambda_s}{\sigma L_s} - \frac{L_m\lambda_r}{\sigma L_s L_r} \tag{5}$$

where $\sigma = (L_s L_r - L_m^2)/(L_s L_r)$.

Under balanced network conditions, the amplitude and rotating speed of the stator flux are constant.

$$\frac{d}{dt}\lambda_s = 0 \tag{6}$$

Neglecting the voltage drop across the stator resistance, the stator voltage equation can be simplified as

$$V_s \approx j\omega_e\lambda_s \tag{7}$$

For SVO, d-axis of the synchronous reference frame (dq) is fixed to the stator voltage ($V_{sq} = 0$, $V_{sd} = V_s$), the stator flux components in the d–q reference frame can be expressed as [3]

$$\lambda_{sd} = 0, \quad \lambda_{sq} = -V_{sd}/\omega_e, \tag{8}$$

The stator apparent power can be calculated as

$$S_s = P_s + jQ_s = -\frac{3}{2}V_s \times \hat{I}_s \tag{9}$$

where $\hat{I}_s$ is the conjugated space vector of I_s. Splitting the previous equation into real and imaginary parts yields

$$P_s = k_\sigma V_{sd}\lambda_{rd}, \quad Q_s = -k_\sigma V_{sd}\left(\lambda_{rq} + \frac{L_r V_{sd}}{L_m\omega_e}\right) \tag{10}$$

where $k_\sigma = \frac{3L_m}{2\sigma L_s L_r}$.

From (10), the rotor fluxes in the dq reference frame are calculated as

$$\lambda_{rd} = \frac{P_s}{k_\sigma V_{sd}}, \quad \lambda_{rq} = -\frac{Q_s}{k_\sigma V_{sd}} - \frac{L_r V_{sd}}{L_m\omega_e} \tag{11}$$

4. Design of total sliding mode controller

The sliding mode strategy is based on the design of the discontinuous control signal that drives the system states toward special manifolds in state space. The manifolds are chosen in such a way that the system will have the desired behavior as the state converges to it [16]. The TSMC is designed to generate the rotor voltage reference components from the stator active and reactive power errors. Two integral switching functions are selected for active and reactive power control. The reference rotor voltage is estimated based on the selected two integral switching functions.

The switching functions of the active and reactive powers are chosen as

$$S = K_p e + K_i \int_0^t e dt \tag{12}$$

where $S = [S_P \quad S_Q]^T$, $e = [e_P \quad e_Q]^T$, $e_P = P_s^* - P_s$, $e_Q = Q_s^* - Q_s$,

K_p and K_i are positive gains, and P_s and Q_s are the actual values of the stator real and reactive powers which can be estimated from the measured stator voltage and current signals.

The time differentiation of the sliding surfaces can be expressed as follows:

$$\dot{S} = K_p\dot{e} + K_i e \tag{13}$$

From (10), time derivative of the stator active and reactive power can be calculated as:

$$\frac{dP_s}{dt} = k_\sigma V_{sd}\frac{d\lambda_{rd}}{dt}, \quad \frac{dQ_s}{dt} = -k_\sigma V_{sd}\frac{d\lambda_{rq}}{dt} \tag{14}$$

From (3), the time derivative of the rotor flux components can be expressed as:

$$\begin{aligned}\frac{d\lambda_{rd}}{dt} &= V_{rd} - R_{rd}I_{rd} + \omega_s\lambda_{rq}\\ \frac{d\lambda_{rq}}{dt} &= V_{rq} - R_{rq}I_{rq} - \omega_s\lambda_{rd}\end{aligned} \tag{15}$$

Combining 10, 11, 14 and 15, neglecting stator resistance voltage drop, time derivative of the sliding surfaces yields

$$\dot{S} = M + F - Du \tag{16}$$

where $\dot{S} = \begin{bmatrix}\dot{S}_P\\ \dot{S}_Q\end{bmatrix}$, $M = \begin{bmatrix}K_i e_P + K_p\dot{P}^*_S\\ K_i e_Q + K_p\dot{Q}^*_S\end{bmatrix}$, $F = K_p\omega_s\begin{bmatrix}Q_s + \frac{L_r V_{sd}}{L_m\omega_e}\\ -P_s\end{bmatrix}$, $D = K_pK_\sigma V_{sd}$, and $u = \begin{bmatrix}-V_{rd}\\ V_{rq}\end{bmatrix}$

System uncertainties occur due to the deviation of the machine parameters from their nominal values and external disturbance. Taking these uncertainties into account, (16) can be rewritten as:

$$\dot{S} = M + F_n - D_n u + W \tag{17}$$

where D_n and F_n are the nominal values of D and F, respectively. W is the lumped uncertainty which can be expressed as:

$$W = \begin{bmatrix}W_P\\ W_Q\end{bmatrix} = \Delta F + \Delta D u \tag{18}$$

The control effort law of the SMC (the reference stator voltage u^*) can be selected to satisfy this condition $\dot{S} = 0$, this yield

$$u^* = D_n^{-1}(M + F_n + \alpha sign(S)) \tag{19}$$

where $\alpha \geqslant |W|$, $\alpha = \begin{pmatrix}\alpha_P\\ \alpha_Q\end{pmatrix}$, $u^* = \begin{bmatrix}V^*_{rd} & V^*_{rq}\end{bmatrix}^T$ and α_P, α_Q are positive gains.

The highly nonlinear and coupled dynamics of the matrices (D_n^{-1}, F_n) complicate the design of the SMC. The variables of these matrices can be analyzed as bounded disturbances regulating the stator active and reactive power. So, it can be added to the lumped uncertainties. The control effort can be rewritten as follows:

$$u^* = M_1 + \alpha_1 sign(S) \tag{20}$$

where $M_1 = D_n^{-1}M$ and $\alpha_1 = |D_n^{-1}(F_n + \alpha)|$

The control effort is designed such that the system trajectory is forced toward the sliding surface ($S = 0$), however, the sensitivity of the controlled system to uncertainties still exists in the reaching phase. To overcome this problem, the TSMC idea is chosen [25], where the control effort can be written as:

$$u^* = M_1 + \alpha_1\, sat(S) + K_c S + \begin{bmatrix}K_P P_s\\ K_Q Q_s\end{bmatrix} \tag{21}$$

where $sat(S) = \frac{S}{|S|+\lambda}$, K_P, K_Q, K_c and λ are positive gains.

The function $sat(S)$ may be used instead of the function $sign(S)$ to reduce the chattering in the control effort. The third and fourth terms are added into (21) to insure the stability of the TSMC during reaching phase. The stability of the proposed TSMC is proved using Lyapunov stability theorem in the Appendix. It is shown that, the estimation of TSMC control effort (21) does not need machine parameter values. The reference rotor voltage can be transformed into the rotor reference frame as

$$V^*_{rabc} = V^*_{rdq}e^{j(\theta_e - \theta_r)} \tag{22}$$

5. Direct power control of GSC

The equivalent circuit of the GSC in dq-synchronous reference frame is shown in Fig. 3 [26,27]. Similar to the flux linkage in DFIGs, stator flux (λ_s) and converter flux (λ_g) can be defined as

$$\lambda_s = \int V_s dt \tag{23}$$

$$\lambda_g = \int V_g dt \tag{24}$$

In dq-synchronous reference frame, (23) and (24) can be expressed as

$$V_s = \dot{\lambda}_s + j\omega_e\lambda_s \tag{25}$$

$$V_g = \dot{\lambda}_g + j\omega_e\lambda_g \tag{26}$$

The relationship between the two fluxes can be given as

$$\lambda_s = L_g I_g + \lambda_g \tag{27}$$

where L_g and I_g are the inductance and current of GSC, respectively. The instantaneous active and reactive power of GSC can be expressed as:

$$P_g + jQ_g = -\frac{3}{2}V_s \times \hat{I}_g \tag{28}$$

where $\hat{I}_g$ is the conjugated space vectors of I_g. Using (27) and (28), the GSC's powers can be estimated as

$$P_g + jQ_g = -\frac{3}{2}V_s \times \frac{1}{L_g}(\hat{\lambda}_s - \hat{\lambda}_g) \tag{29}$$

Decomposing the active and reactive power of the GSC yields

$$P_g = \frac{3}{2L_g}V_{sd}\lambda_{gd}, \quad Q_g = -\frac{3}{2L_g}V_{sd}\left(\lambda_{gq} + \frac{V_{sd}}{\omega_e}\right) \tag{30}$$

The time derivative of the active and reactive power can be expressed as follows:

$$\frac{dP_g}{dt} = \frac{3V_{sd}}{2L_g}\frac{d\lambda_{gd}}{dt}, \quad \frac{dQ_g}{dt} = -\frac{3V_{sd}}{2L_g}\frac{d\lambda_{gq}}{dt} \tag{31}$$

Over a constant sample time (Ts), the active and reactive power variation can be expressed as

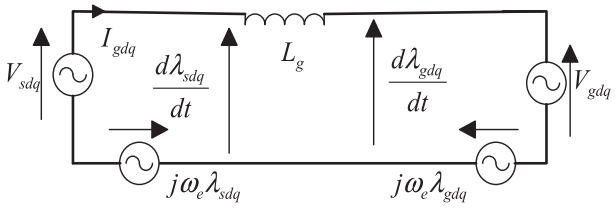

Figure 3 Equivalent circuit of the GSC.

$$\Delta P_g = \frac{3V_{sd}}{2L_g}\Delta\lambda_{gd}, \qquad \Delta Q_g = -\frac{3V_{sd}}{2L_g}\Delta\lambda_{gq} \tag{32}$$

where $\Delta P_g^* = P_g^* - P_g$ and $\Delta Q_g^* = Q_g^* - Q_g$.

The GSC active power reference (P_g^*) is estimated as

$$P_g^* = (k_{pv} + k_{dv}s + \frac{k_{iv}}{s})(V_{dc}^* - V_{dc}) \tag{33}$$

where k_{pv}, k_{dv} and k_{iv} are the proportional, differential and integral gains of the PID controller, respectively.

From (26), the reference GSC voltages, over a constant sample time (Ts), can be estimated as follows

$$V_{gdq}^* = \Delta\lambda_{gdq}/T_s + j\omega_e\lambda_{gdq} \tag{34}$$

Substituting (30) and (32) into (34), the reference GSC voltage can be expressed as follows:

$$\begin{aligned} V_{gd}^* &= \frac{2L_g\Delta P_g}{3V_sT_s} + \frac{2L_g\omega_eQ_g}{3V_s} + V_{sd} \\ V_{gq}^* &= -\frac{2L_g\Delta Q_g}{3V_sT_s} + \frac{2L_g\omega_eP_g}{3V_s} \end{aligned} \tag{35}$$

6. System implementation

The block diagram of the proposed DPC strategy is given in Fig. 4. Three phase stator voltages and currents are measured and transformed into a stator stationary reference frame. For RSC, the stator output active and reactive powers are calculated from the measured stator voltage and current signals. The rotor voltage reference values are estimated using TSMC controller. Finally, a pulse width modulation (PWM) technique is used to provide the switching patterns of the RSC with a constant switching frequency. For GSC, the active and reactive power values are calculated using the measured stator voltage and GSC current. The reference value of the GSC voltage is estimated using (35). It is shown that the proposed schemes are less complicated compared with other control algorithms such as vector or field oriented control, where the current control loops and axes transformation of the voltage and current are totally eliminated. Moreover, PI-controllers of RSC and GSC are not required.

7. Simulation results

Simulations of the proposed control strategies for a DFIG-based wind generation are conducted by using the Matlab/Simulink package. The DFIG is rated at 1.5 MW, and its parameters are listed in Table 1. Fig. 5 shows the schematic diagram of the tested system. The nominal dc-link voltage is 1200 V, and the switching frequencies for both converters are 3 kHz. As shown in Fig. 5, a high-frequency AC filter is shunt connected to the stator side to absorb the switching harmonics generated by the two converters. The parameters of the proposed total sliding mode controller are selected to provide optimum performance as: $K_i = 5$, $K_p = 0.1$, $K_c = 0.1$, $K_P = 1$, $K_Q = 1$, $\alpha = [5\ 5]$. For GSC, the proportional, differential and integral gains of the PID controller are $k_{pv} = 0.5$, $k_{iv} = 50$, $k_{dv} = 0.05$.

Case (1): In this case, the performance of the conventional [11] and proposed TSMC schemes is tested under reference

Table 1 Parameters of the simulated DFIG.

Rated power	1.5 MW	$L_{\sigma s}$	0.171 pu
Stator voltage	575 V/60 Hz	$L_{\sigma r}$ (referred to the stator)	0.156 pu
Stator/rotor turns ratio	0.38	L_m	2.9 pu
R_s	0.0071 pu	Lumped inertia constant	5.04 s
R_r (referred to the stator)	0.005 pu		

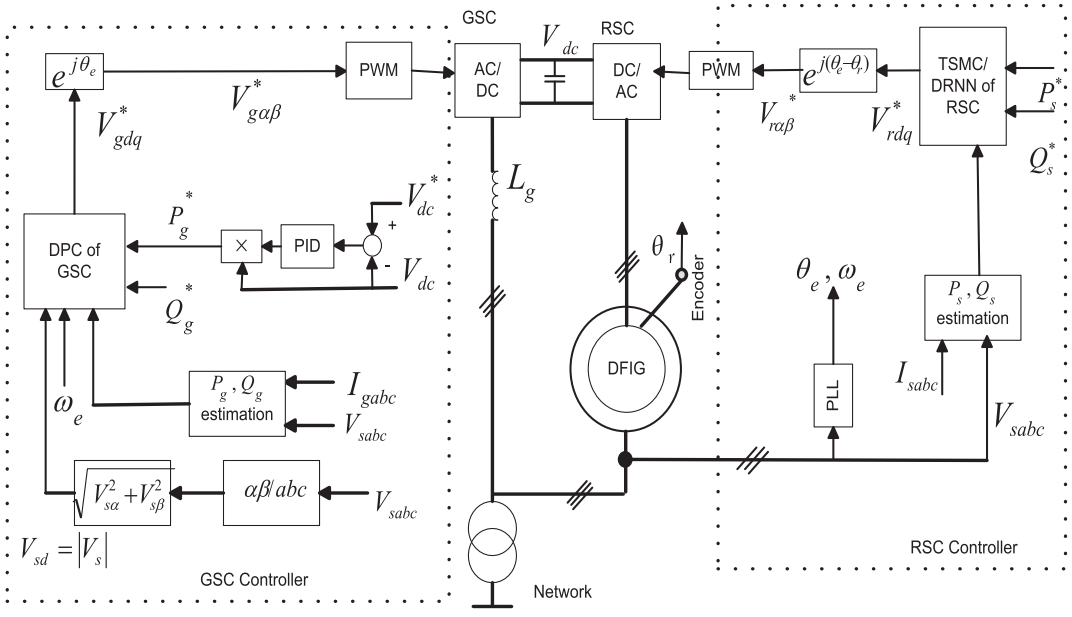

Figure 4 Block diagram of the DPC of a DFIG under balanced network conditions.

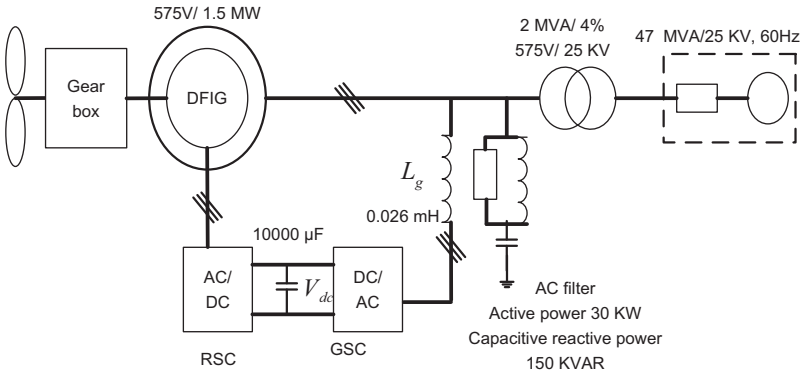

Figure 5 Schematic diagram of the tested system.

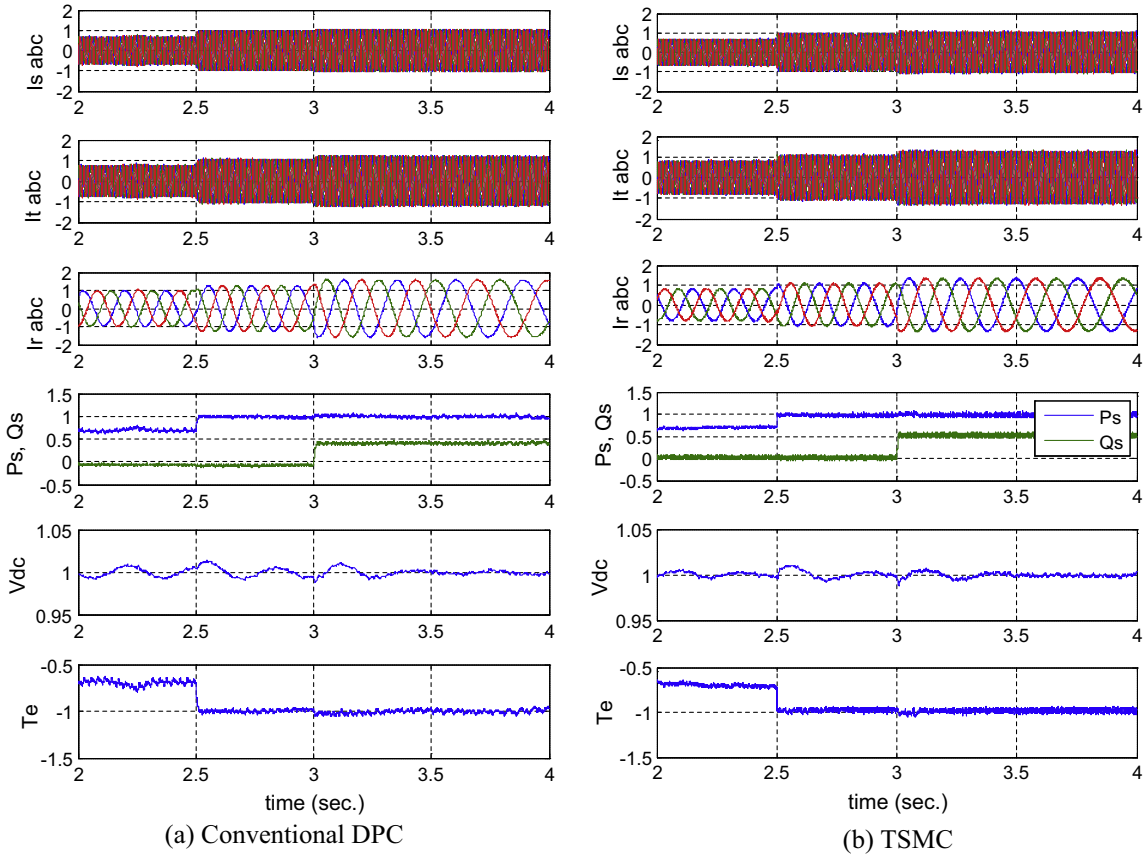

Figure 6 Performance of the conventional and TSMC direct power controllers with power references variation.

power variation. In [11], the RSC is controlled based on conventional DPC scheme, while the GSC is controlled based on vector control. The rotor speed is assumed to be constant at 1.1 p.u. The reference values of stator active and reactive powers are set at 0.7 and 0 p.u., respectively. At $t = 2.5$ s, the stator active power reference value is assumed to be changed to 1 p.u. At $t = 3$ s, the stator reactive power reference value is changed to 0.5 p.u. Fig. 6 shows the results of the conventional DPC and TSMC, respectively, under the described operating conditions. The figure shows the waveforms of the stator current (I_{sabc}), total current (I_{tabc}), rotor current (I_{rabc}), stator active power (P_s) (blue line), stator reactive power (Q_s) (green line), dc-link voltage (V_{dc}) waveforms and electromagnetic torque (T_e), respectively. All the values are given in per unit. The waveforms are enlarged from 2 to 4 s for better illustrations. It is shown that the TSMC controller has high performance compared to the conventional DPC. The PID controller could regulate well the DC-link voltage where no oscillations appear in the power and DC-link voltage waveforms of the TSMC compared to the conventional DPC. The decoupling control of the stator active and reactive power is achieved. The electromagnetic torque of the proposed scheme has low ripples especially at low power command. The power waveforms of the two schemes are enlarged in Fig. 7. The results show that the

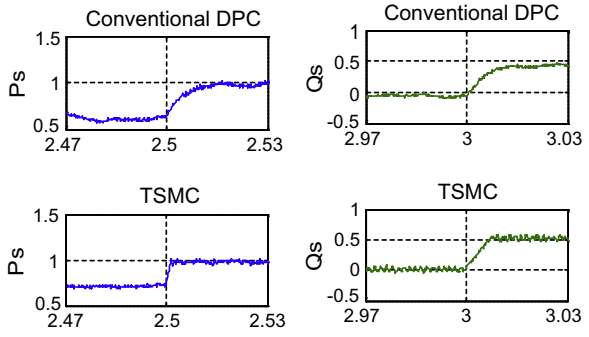

Figure 7 Enlarged power waveforms of the conventional DPC and TSMC controllers.

TSMC controller has fast transient response. It is clear from the results that the TSMC controller has satisfied performance.

Case (2): In this case, the performance of the proposed scheme is tested under wind speed, machine parameters and stator reactive power variation. The rotor speed is changed from 0.9 to 1.1 p.u. during one second (from 3 to 4 s.). The DFIG is operated in a maximal power tracking mode, where its active power is controlled according to the optimal speed curve [11]. The reactive power reference is changed from 0 to 0.5 p.u. at $t = 3$ s. The stator and rotor resistance of the DFIG are assumed to be increased due to heating by 50% and the magnetizing inductance is decreased by 50% due to saturation. In this test, the lumped inertia constant of the system is set to a relatively small value of 0.5 s for a better illustration. Fig. 8 shows the simulation results of the TSMC under the described conditions. The figure shows the waveforms of the stator current (I_{sabc}), total current (I_{tabc}), rotor current (I_{rabc}), stator active power (P_s), stator reactive power (Q_s), GSC active power (P_g), GSC reactive power (Q_g), dc-link voltage (V_{dc}), electromagnetic torque (T_e) and rotor speed (w_r) waveforms, respectively. It is shown that the decoupled control of the stator active and reactive powers is achieved under sub-synchronous or super-synchronous operation. The controllers can transfer smoothly from sub-synchronous to super-synchronous speed operation. Small oscillations appear in the power waveforms as a result of a low inertia. Actually, the high inertia of the turbine and generator could damp these oscillations. In spite of parameters variation, the stator active and reactive powers can track well the reference values.

Case (3): In this case, the performance of the TSMC is tested under unbalanced grid voltage conditions. Single phase voltage unbalance (10%) is assumed to be occurred at 2.5 s [24]. The stator and rotor resistance of the DFIG are assumed to be increased due to heating by 50% and the magnetizing inductance is decreased by 50% due to saturation. The rotor speed is changed from 1.05 to 0.95 p.u. during 2.5 s. The reference values of the stator active and reactive powers are 1 and 0 p.u., respectively. The simulation results of the proposed scheme are shown in Fig. 9. The results show that the three phase stator voltage, stator current, total current and the rotor current waveforms have

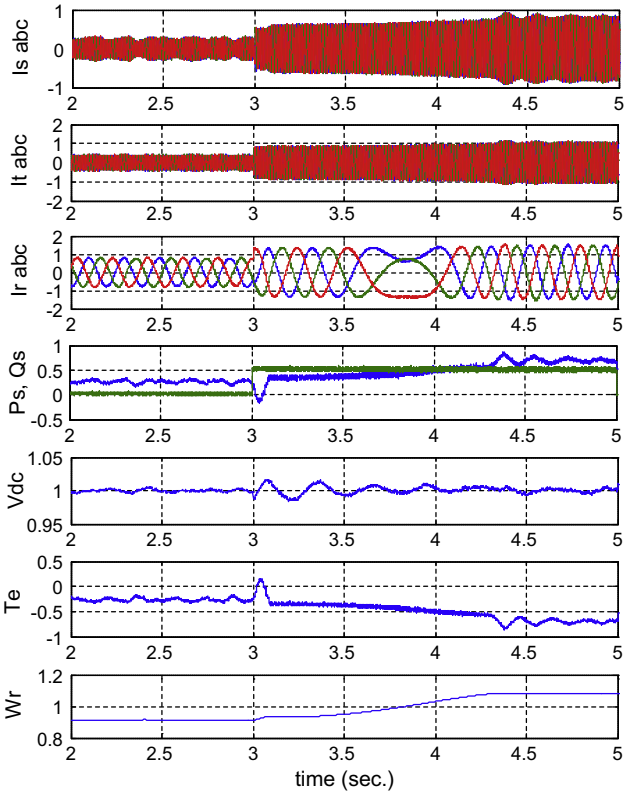

Figure 8 Performance of the TSMC during wind speed, reactive power and parameters variation.

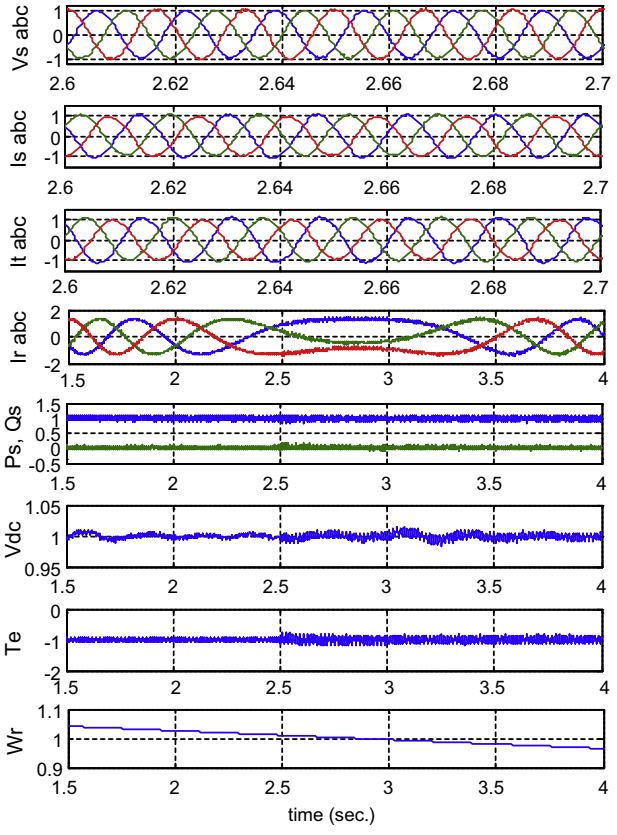

Figure 9 Performance of the TSMC during wind speed, parameters variation and unbalanced grid voltage (10%).

low harmonics. The stator active and reactive powers, DC-link voltage and electromagnetic torque waveforms have low oscillations. These oscillations decrease as the slip angular speed ($\omega_s = \omega_e - \omega_r$) increases.

8. Conclusion

In this paper, a robust scheme is proposed to improve the performance of the DPC of the DFIG driven by variable speed wind turbine. Total sliding mode controller is designed to replace the conventional DPC. TSMC is designed to generate the switching state of the RSC based on the stator active and reactive power errors. In addition, the GSC is controlled based on DPC to regulate the dc-link voltage and reactive power. The proposed scheme preserves the advantages of the classical DPC such as simplicity and less parameters dependence. The performance of conventional and proposed schemes is studied under wind speed, machine parameters, power reference variation and unbalanced voltage grid conditions. By comparing the performance of the proposed scheme with conventional DPC, it can conclude that the proposed scheme has fast transient response under reference power variation conditions. The proposed scheme has superior performance under sub- and super-synchronous speed operation even with parameters variation. Moreover, under unbalanced grid voltage condition operation, the stator, rotor and total currents have very low harmonics content. In addition, the DC-link voltage, electromagnetic torque, stator active and reactive power waveforms have small oscillations.

Appendix A

Stability of the proposed SMC

The stability of the proposed SMC can be proved using Lyapunov stability theorem.

Define Lyapunov function as follows:

$$V = \frac{1}{2} s^T s \tag{A.1}$$

The time derivative of V on the state trajectory is given by

$$\dot{V} = s^T \dot{s} \tag{A.2}$$

Substituting (17), the time derivative of V becomes

$$\dot{V} = S^T (M + F_n - D_n u + W) \tag{A.3}$$

By substituting the control effort (19)

$$\dot{V} = s^T W - \alpha |s^T| \tag{A.4}$$

For $\alpha > |W|$, Eq. (A.4) will become:

$$\dot{V} \leqslant 0 \tag{A.5}$$

This proves the stability of the proposed controller.

References

[1] A. Petersson, T. Thiringer, L. Harnefors, T. Petru, Modeling and experimental verification of grid interaction of a DFIG wind turbine, IEEE Trans. Energy Convers. 20 (4) (2005) 878–886.

[2] L. Xu, W. Cheng, Torque and reactive power control of a doubly fed induction machine by position sensorless scheme, IEEE Trans. Ind. Appl. 31 (3) (1995) 636–642.

[3] S. Muller, M. Deicke, R.W. De Doncker, Doubly fed induction generator systems for wind turbines, IEEE Ind. Appl. Mag. 8 (3) (2002) 26–33.

[4] M. Depenbrock, Direct self-control (DSC) of inverter-fed induction machine, IEEE Trans. Power Electron. 3 (4) (1988) 420–429.

[5] I. Takahashi, T. Noguchi, A new quick-response and high-efficiency control strategy of an induction motor, IEEE Trans. Ind. Appl. 22 (5) (1986) 820–827.

[6] R. Datta, V.T. Ranganathan, Direct power control of grid-connected wound rotor induction machine without rotor position sensors, IEEE Trans. Power Electron. 16 (3) (2001) 390.

[7] L. Xu, P. Cartwright, Direct active and reactive power control of DFIG for wind energy generation, IEEE Trans. Energy Convers. 21 (3) (2006) 750–758.

[8] D. Zhi, L. Xu, Direct power control of DFIG with constant switching frequency and improved transient performance, IEEE Trans. Energy Convers. 22 (1) (2007) 110–118.

[9] S. Jou, S. Lee, Y. Park, K. Lee, Direct power control of a DFIG in wind turbines to improve dynamic responses, J. Power Electron. 9 (5) (2009) 781–790.

[10] H. Nian, Y. Song, P. Zhou, Y. He, Improved direct power control of a wind turbine driven doubly fed induction generator during transient grid voltage unbalance, IEEE Trans. Energy Convers. 26 (3) (2011) 976–985.

[11] E.G. Shehata, Direct power control of wind-turbine-driven DFIG during transient grid voltage unbalance, Wind Energy (2013), http://dx.doi.org/10.1002/we.1619.

[12] G. Abad, M.A. Rodŕiguez, G. Iwanski, J. Poza, Direct power control of doubly-fed-induction-generator-based wind turbines under unbalanced grid voltage, IEEE Trans. Power Electron. 25 (2) (2010).

[13] M.V. Kazemi, A.S. Yazdankhah, H.M. Kojabadi, Direct power control of DFIG based on discrete space vector modulation, Renewable Energy 35 (5) (2010) 1033–1042.

[14] D. Santos-Martin, J.L. Rodriguez-Amenedo, S. Arnalte, Direct power control applied to doubly fed induction generator under unbalanced grid voltage conditions, IEEE Trans. Power Electron. 23 (5) (2008) 2328–2336.

[15] E.G. Shehata, Gerges M. Salama, Direct power control of DFIGs based wind energy generation systems under distorted grid voltage conditions, Electr. Power Energy Syst. 53 (2013) 956–966.

[16] V.I. Utkin, Sliding mode control design principles and applications to electric drives, IEEE Trans. Ind. Electron. 40 (1) (1993) 23–36.

[17] S.Z. Chen, N.C. Cheung, K.C. Wong, J. Wu, Integral variable structure direct torque control of doubly fed induction generator, IET Renew. Power Gener. 5 (1) (2011) 18–25.

[18] D. Kairous, R. Wamkeue, DFIG-based fuzzy sliding-mode control Of WECS with a flywheel energy storage, Electr. Power Syst. Res. 93 (2012) 16–23.

[19] V.N. Pande, U.M. Mate, Shailaja Kurode, Discrete sliding mode control strategy for direct real and reactive power regulation of wind driven DFIG, Electr. Power Syst. Res. 100 (2013) 73–81.

[20] S.Z. Chen, N.C. Cheung, K.C. Wong, J. Wu, Integral variable structure direct torque control of doubly fed induction generator under Unbalanced grid voltage, IEEE Trans. Energy Convers. 25 (2) (2010) 356–368.

[21] J. Hu, X. Yuan, VSC-based direct torque and reactive power control of doubly fed induction generator, Renewable Energy 40 (2012) 13–23.

[22] M.I. Martinez, G. Tapia, A. Susperregui, H. Camblong, Sliding mode control for DFIG rotor and grid side converter under balanced and harmonically distorted grid voltage, IEEE Trans. Energy Convers. 27 (2) (2012) 328–339.
[23] L. Shang, J. Hu, Sliding mode based direct power control of grid connected wind turbine driven doubly fed induction generator under unbalanced grid voltage conditions, IEEE Trans. Energy Convers. 27 (2) (2012) 362–373.
[24] Siegfried Heier, Grid Integration of Wind Energy Conversion Systems, John Wiley & Sons Ltd, 1998, ISBN 0-97143-X.
[25] E.G. Sheahta, Speed sensorless torque control of an IPMSM drive with online stator resistance estimation using reduced order EKF, Electr. Power Energy Syst. 47 (2013) 378–386.
[26] L. Xu, D. Zhi, L. Yao, Direct power control of grid connected voltage source converters, in: IEE power engineering annual meeting, pp. 1–6, 2007.
[27] D. Zhi, L. Xu, B. Williams, Improved direct power control of grid-connected DC/AC converters, IEEE Trans. Power Electron. 25 (5) (2009) 1280–1292.